Transit Met Chem (2017) 42:123–130
DOI 10.1007/s11243-016-0114-8

Three-dimensional nickel(II) and cobalt(II) coordination polymers constructed from 2,5-dichloroterephthalic acid and bis(imidazole) ligands

Shao Yun Hao[1] · Zeng Chuan Hao[1] · Ce Liu[1] · Guang Hua Cui[1]

Received: 8 October 2016 / Accepted: 12 December 2016 / Published online: 21 December 2016

Abstract Two ternary mixed-ligand coordination polymers (CPs), namely $[Ni(L)_2(DCTP)]_n$ (**1**) and $[Co(L)(DCTP)]_n$ (**2**), have been hydrothermally synthesized by reacting different transition metal salts with 2,5-dichloroterephthalic acid (H_2-DCTP) and 4,4′-[bis(imidazol-1-ylmethylene)]biphenyl (L) as ligands. Both CPs **1** and **2** were characterized by elemental analysis, IR spectroscopy, and single-crystal X-ray diffraction; CP **1** exhibits a non-interpenetrated six-connected α-Po (or **pcu** net) framework structure, with the point symbol $\{4^{12}\cdot6^3\}$. CP **2** shows a fivefold-interpenetrating four-connected **sqc6** topology with the point symbol $\{6^6\}$. The thermal stabilities, luminescence and catalytic properties of both CPs for the degradation of methyl orange in a Fenton-like process have been investigated.

Introduction

Due to their interesting structures and potential applications in gas storage, molecular recognition, catalysis and magnetism, the design and synthesis of coordination polymers (CPs) are of considerable current interest [1–3]. The structural diversities of CPs may be tuned by a suitable choice of metal ions as well as ligands. With regard to the latter, variations in backbone flexibility, size, substituents, and symmetry of organic linkers can result in CPs with a wide range of structures and properties [4–6]. The most generally employed strategies for synthesis of CPs are the use of (a) neutral spacers to enhance the possibility of increasing the dimensionality of CPs, with charge neutrality maintained by non-coordinating anions; and (b) anionic bridging ligands, which can partially or fully counterbalance the charges of the metal centers. Therefore, rational selection of organic ligands based on their flexibility, functionality, shape, and symmetry plays a significant role in modulating structures and properties of CPs [7–9]. One of the most commonly effective routes for building such networks is to employ appropriate bridging ligands that can bind metal ions in different modes and so provide a possible route to novel CPs with intriguing structures and topological features [10].

In this field, polycarboxylates have been widely employed to manipulate coordination networks, in view of their versatile coordination modes and acidic nature [11]. In particular, terephthalic acid is one of the most popular rod-like building blocks that have been widely used to construct functional CPs [12]. However, research on the analogous halogenated terephthalic acids, with disparate steric and electronic effects, has been insufficiently unexplored so far [13–15]. In addition, CPs with open coordination sites have attracted much attention, and the incorporation of halogen atoms into carboxylate ligands may be an effective way to construct CPs with open coordination sites because of a diminished possibility for a priori structure prediction or crystal design [16]. Meanwhile, semi-flexible bis(imidazole) derivatives which can utilize diverse conformations to accommodate different metal centers have been extensively used as auxiliary

Electronic supplementary material The online version of this article (doi:10.1007/s11243-016-0114-8) contains supplementary material, which is available to authorized users.

✉ Guang Hua Cui
tscghua@126.com

[1] College of Chemical Engineering, Hebei Key Laboratory for Environment Photocatalytic and Electrocatalytic Materials, North China University of Science and Technology, Tangshan 063009, Hebei, People's Republic of China

N-donor ligands in the synthesis of mixed-ligand CPs [17, 18].

To explore the influence of different transition metal salts on the final structures and properties of such CPs, we have successfully synthesized two new CPs under the same reaction conditions, formulated as $[Ni(L)_2(DCTP)]_n$ (**1**) and $[Co(L)(DCTP)]_n$ (**2**) [L = 4,4′-(bis(imidazol-1-yl-methylene))biphenyl, H_2DCTP = 2,5-dichloroterephthalic acid]. These two CPs have totally different structures; CP **1** exhibits a 3D six-connected framework, while CP **2** reveals a 3D four-connected network.

Experimental

Materials and methods

The free ligand L was synthesized by the literature method [19]. The other reagents and solvents were purchased from commercial sources and used without further purification. Elemental analyses (C, N and H) were obtained on a PerkinElmer 240C elemental analyzer. A Varian FT-IR 640 spectrophotometer was employed for collection of IR spectra (using KBr pellets in the range of 4000–400 cm^{-1} region). The luminescence spectra of powdered solid samples were measured at room temperature, using a Hitachi F-7000 fluorescence spectrophotometer. Solid-state UV/Vis diffuse reflectance spectra were measured using a UV–Vis spectrophotometer (Puxi, UV 1901), and a $BaSO_4$ plate was employed as the reflectance standard. X-ray powder diffraction (XRPD) patterns were obtained on a Rigaku D/Max-2500 diffractometer at 40 kV, 100 mA with a graphite monochromator and Cu-target tube (λ = 1.5406 nm). A NETZSCH TG 209 thermal analyzer was applied to record thermal curves under N_2 atmosphere from room temperature to 800 °C with a heating rate of 10 °C/min. The absorptivity value of methyl orange (MO) was measured at the maximum wavelength of 506 nm with a Shanghai Jingke 722N spectrophotometer.

Synthesis of $[Ni(L)_2(DCTP)]_n$ (1)

A mixture of $Ni(OAc)_2{\cdot}4H_2O$ (24.9 mg, 0.1 mmol), the free ligand L (31.4 mg, 0.1 mmol), H_2DCTP (23.5 mg, 0.1 mmol), and distilled water (10 mL) was charged into a Teflon-lined stainless vessel and heated from room temperature to 140 °C for 72 h and then cooled to room temperature at a rate of 5 °C/h. The resulting crystals were filtered out, washed with small quantities of cold distilled water and dried overnight, giving green block crystals. Yield, 47.7% referred to $Ni(OAc)_2{\cdot}4H_2O$. Anal. Calc. for $C_{48}H_{38}NiCl_2N_8O_4$ (M_r = 920.47): C, 62.6; H, 4.2; N, 12.2%. Found: C, 62.6; H, 4.2; N, 12.2%. IR (KBr, cm^{-1}): 3033w, 2966m, 1639m, 1578s, 1352w, 1233w, 1034s, 773w, 659m, 568s, 498w.

Synthesis of $[Co(L)(DCTP)]_n$ (2)

The method of synthesis for CP **2** was similar to that for CP **1**, except that $Co(OAc)_2{\cdot}4H_2O$ (24.9 mg, 0.1 mmol) was used instead of $Ni(OAc)_2{\cdot}4H_2O$. Red block crystals of **2** were obtained with a yield of 42.6% [based on $Co(OAc)_2{\cdot}4H_2O$]. Anal. Calc. for $C_{28}H_{20}CoCl_2N_4O_4$ (M_r = 606.31): C, 55.47; H, 3.32; N, 9.24%. Found: C, 55.5; H, 3.3; N, 9.3%. IR (KBr, cm^{-1}): 2924m, 1592s, 1520s, 1443w, 1369s, 1233s, 1105w, 823m, 741s, 658m, 578w, 496m.

X-ray crystallography

Suitable single crystals of CPs **1** and **2** were selected for single-crystal X-ray diffraction analyses. The intensity data for both CPs were collected with a Bruker Smart CCD diffractometer with Mo–K_α radiation (λ = 0.71073 Å) using ω scan mode at 296(2) K. The multiscan program [20] was employed to collect the absorption corrections. The structures were solved by direct methods applying the SHELXS-2014 program and refined through full-matrix least-squares on F^2 using the SHELXTL program package [21]. Hydrogen atoms of the organic parts were located from difference maps and refined with isotropic temperature factors, and the anisotropic thermal parameters were refined for non-hydrogen atoms. Metal atoms in both CPs were located in the E-maps. The detailed crystallographic data and structure refinement parameters for both CPs are given in Table 1.

Catalysis experiments

In order to assess the potential of these CPs as catalysts for the oxidation of MO, the following procedure was followed: briefly $Na_2S_2O_8$ (25.0 mg) was placed in a 150-mL round-bottom flask and dissolved in 100.0 mL of an aqueous solution of MO (10 mg/L). The pH was adjusted to 3.0 using 0.1 mol/L H_2SO_4, and finally a powdered sample of the required CP (30.0 mg) was added. The mixture was stirred magnetically at a constant temperature of 30 °C. Aliquots (5.0 mL) of the reaction solution were removed at given time intervals and centrifuged to remove the residual catalyst and then analyzed with a Shanghai Jingke 722N visible spectrophotometer at 506 nm. A control experiment was carried out in the absence of either CP under the same conditions. The degradation efficiency of MO was evaluated based on the following formula [22]:

Table 1 Crystal and refinement data for CPs **1** and **2**

CPs	**1**	**2**
Chemical formula	$C_{48}H_{38}Cl_2N_8NiO_4$	$C_{28}H_{20}Cl_2CoN_4O_4$
Formula weight	920.47	606.31
Crystal system	Monoclinic	Monoclinic
Space group	*P*2(1)/*c*	*C*2/*c*
a (Å)	11.530(5)	18.209(4)
b (Å)	21.684(9)	6.913(2)
c (Å)	8.452(4)	20.445(4)
α (°)	90	90
β (°)	103.405(6)	98.156(3)
γ (°)	90	90
V (Å^3)	2055.6(15)	2547.8(9)
Z	2	4
D_{calcd} (g/cm^3)	1.487	1.581
Absorption coefficient (mm^{-1})	0.661	0.928
F(000)	952	1236
Crystal size (mm)	0.22 × 0.22 × 0.20	0.25 × 0.24 × 0.22
θ range (°)	2.044–27.474	2.013–27.440
Index range *h*, *k*, *l*	−14/14, −28/28, −10/10	−23/23, −8/8, −26/20
Reflections collected	18,494	7465
Max. and min. transmission	0.9049, 0.8812	0.8813, 0.8029
Data/restraint/parameters	4693/0/286	2880/500/280
Goodness of fit on F^2	1.092	1.107
Final R_1, wR_2 [$I > 2\sigma(I)$]	0.0524, 0.1363	0.0621, 0.1686
Largest diff. peak and hole	0.559, −0.661	0.611, −0.808

$$\text{Degradation efficiency} = [(A_0 - A_t)/A_0] \times 100\%$$

where A_0 is the initial absorbance of MO aqueous solution and A_t (mg/L) is the absorbance at reaction time *t*. The MO concentration was below 10 mg/L and was linearly proportional to the intensity of the measured peak.

Results and discussion

General characterization of the CPs

The hydrothermal approach plays a significant role in the self-assembly of CPs. By varying the metal salt, single crystals of CPs **1** and **2** were successfully obtained. Both CPs are stable in the solid state and insoluble in water and common organic solvents, such as dichloromethane, alcohol, benzene and acetonitrile. In addition, both CPs were structurally characterized by X-ray single-crystal diffraction analysis. Selected bond distances and angles for the CPs are listed in Table 2.

Crystal structure of CP 1

X-ray single-crystal diffraction analysis reveals that CP **1** formulated as $[Ni(L)_2(DCTP)]_n$ crystallizes in the monoclinic *P*2(1)/*c* space group. The asymmetric unit contains half of an Ni(II) atom, one L ligand, and half of a $DCTP^{2-}$ ligand. As illustrated in Fig. 1a, the nickel center has an ideal $[NiO_2N_4]$ octahedral geometry, provided by two oxygen atoms (O1, O1A, symmetry code: $A = -x + 2, -y + 1, -z + 1$) from carboxylate groups belonging to two distinct $DCTP^{2-}$ ligands and four nitrogen atoms (N1B, N1C, N4, N4A, symmetry codes: $B = x + 1, -y + 1/2, z + 1/2$; $C = -x + 1, y + 1/2, -z + 1/2$) from four distinct L ligands. The values of the Ni–O bond distances are 2.097(2) Å, and the two pairs of Ni–N bond distances are 2.102(3) and 2.103(3) Å, respectively. These values are all in the normal ranges according to the literature [23].

In CP **1**, each anionic $DCTP^{2-}$ ligand adopts a $(\kappa^1\text{–}\kappa^0)\text{–}(\kappa^1\text{–}\kappa^0)\text{–}\mu_2$ coordination mode to link adjacent Ni(II) centers into a 1D linear chain, with an Ni···Ni distance of 11.530(5) Å. The ligand L adopts a *trans*-conformation to connect the Ni atoms into a 2D reticular layer (Fig. S1). The dihedral angle between two imidazole arms of each entire ligand L is 65.78°, while the Ni···Ni distance is 15.677(5) Å. The reticular 2D layers and 1D linear chains are interlaced with each other to generate an intricate 3D network (as shown in Fig. 1b). In order to better understand the structure of CP **1**, topological analysis of the intricate network was performed using TOPOS

Table 2 Selected bond lengths (Å) and angles (°) for CPs **1** and **2**

Parameter	Value	Parameter	Value
1			
Ni(1)–O(1)	2.097(2)	Ni(1)–O(1)A	2.097(2)
Ni(1)–N(1)B	2.103(3)	Ni(1)–N(1)C	2.103(3)
Ni(1)–N(4)	2.104(3)	Ni(1)–N(4)A	2.104(3)
O(1)–Ni(1)–O(1)A	180.0	N(1)B–Ni(1)–N(4)	87.82(11)
O(1)–Ni(1)–N(1)B	86.29(10)	N(1)C–Ni(1)–N(4)	92.18(11)
O(1)A–Ni(1)–N(1)B	93.71(10)	O(1)–Ni(1)–N(4)A	86.59(9)
O(1)–Ni(1)–N(1)C	93.71(10)	O(1)A–Ni(1)–N(4)A	93.42(9)
O(1)A–Ni(1)–N(1)C	86.29(10)	N(1)B–Ni(1)–N(4)A	92.18(11)
N(1)B–Ni(1)–N(1)C	180.0	N(1)C–Ni(1)–N(4)A	87.82(11)
O(1)–Ni(1)–N(4)	93.41(9)	N(4)–Ni(1)–N(4)A	180.0
O(1)A–Ni(1)–N(4)	86.58(9)		
2			
Co(1)–O(1)	1.896(4)	Co(1)–O(1)A	1.896(4)
Co(1)–N(1)	1.948(10)	Co(1)–N(1)A	1.948(10)
O(1)–Co(1)–O(1)A	129.3(4)	O(1)–Co(1)–N(1)	117.0(4)
O(1)A–Co(1)–N(1)	86.7(3)	O(1)A–Co(1)–N(1)A	117.0(3)
N(1)–Co(1)–N(1)A	124.9(5)	O(1)–Co(1)–N(1)A	86.7(3)

Symmetry codes for **1**: A: $-x + 2$, $-y + 1$, $-z + 1$; B: $x + 1$, $-y + 1/2$, $z + 1/2$; C: $-x + 1$, $y + 1/2$, $-z + 1/2$; D: $-x + 1$, $-y + 1/2$, $-z + 1/2$; for **2**: A: $-x + 1$, y, $-z + 3/2$; B: $-x + 1$, $-y$, $-z + 1$

4.0 software [24]. The Ni(II) center can be simplified as six-connected, and the anionic $DCTP^{2-}$ ligands and L ligands as linkers. The structure of the CP **1** can then be represented as a six-connected α-Po (or **pcu** net) primitive cubic net with the point symbol $\{4^{12}\cdot6^3\}$. The cubic pore dimensions are approximately 15.677 × 15.677 × 11.530 $Å^3$ (as shown in Fig. S2).

Crystal structure of CP 2

X-ray single-crystal diffraction analysis shows that CP **2** formulated as $[Co(L)(DCTP)]_n$ crystallizes in the monoclinic *C*2/*c* space group. The asymmetric unit is composed of half of a Co(II) center, half of a L ligand, and half of a $DCTP^{2-}$ ligand. As shown in Fig. 2a, the Co(II) centers are four-coordinated in a distorted $[NiO_2N_2]$ tetrahedral geometry provided by carboxyl oxygen atoms from two different $DCTP^{2-}$ ligands [Co(1)–O(1) = 1.896(4) Å, Co(1)–O(1)A = 1.896(4) Å, symmetry code: A = –$x + 1$, y, $–z + 3/2$; B = $-x + 1$, $-y$, $-z + 1$] plus two nitrogen atoms from two disparate L ligands [Co(1)–N(1) = 1.948(10) Å, Co(1)–N(1)A = 1.948(10) Å]. These values are all in the normal ranges according to the previous reports [25].

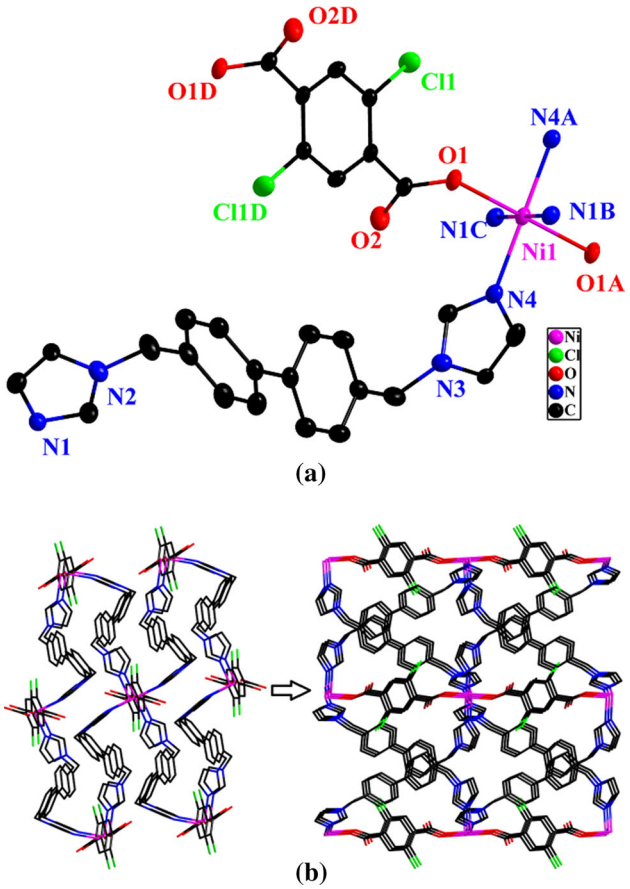

Fig. 1 **a** Coordination environment around the Ni(II) centers in CP **1**. Hydrogen atoms are omitted for clarity (symmetry codes: A: $-x + 2$, $-y + 1$, $-z + 1$; B: $x + 1$, $-y + 1/2$, $z + 1/2$; C: $-x + 1$, $y + 1/2$, $-z + 1/2$; D: $-x + 1$, $-y + 1/2$, $-z + 1/2$). **b** The 3D network of CP **1** constructed by Ni(II) centers, L ligands, and $DCTP^{2-}$ ligands

In CP **2**, the anionic $DCTP^{2-}$ ligands employ a $(\kappa^1–\kappa^0)–(\kappa^1–\kappa^0)–\mu_2$ coordination mode to connect the neighboring Co atoms into a 1D wave-like chain with a Co···Co distance of 11.013(2) Å and Co···Co···Co angle of 136.3(3)°. In addition, the ligand L acts as an μ_2 liker which adopts *trans*-conformation to link the contiguous Co atoms into a 1D "W"-like chain with a somewhat longer Co···Co separation of 18.230(3) (Fig. S3). Furthermore, the 1D wave-like chains and "W"-like chains interact with each other to construct a 3D circularly heart-shaped framework (as shown in Fig. 2b). The topological method was used to study the nature of the resulting 3D structure. Thus, the Co(II) atoms can be simplified as four-connected, and the L and $DCTP^{2-}$ ligands as linkers. In this way, the intricate 3D structure can be represented as a uninodal four-connected **sqc6** topological network with the point symbol $\{6^6\}$. The potential spaces are large enough to be filled via mutual interpenetration of five independent 3D networks, generating a fivefold-interpenetrating 3D structure (as shown in Fig. S4). The interpenetration can be classified as

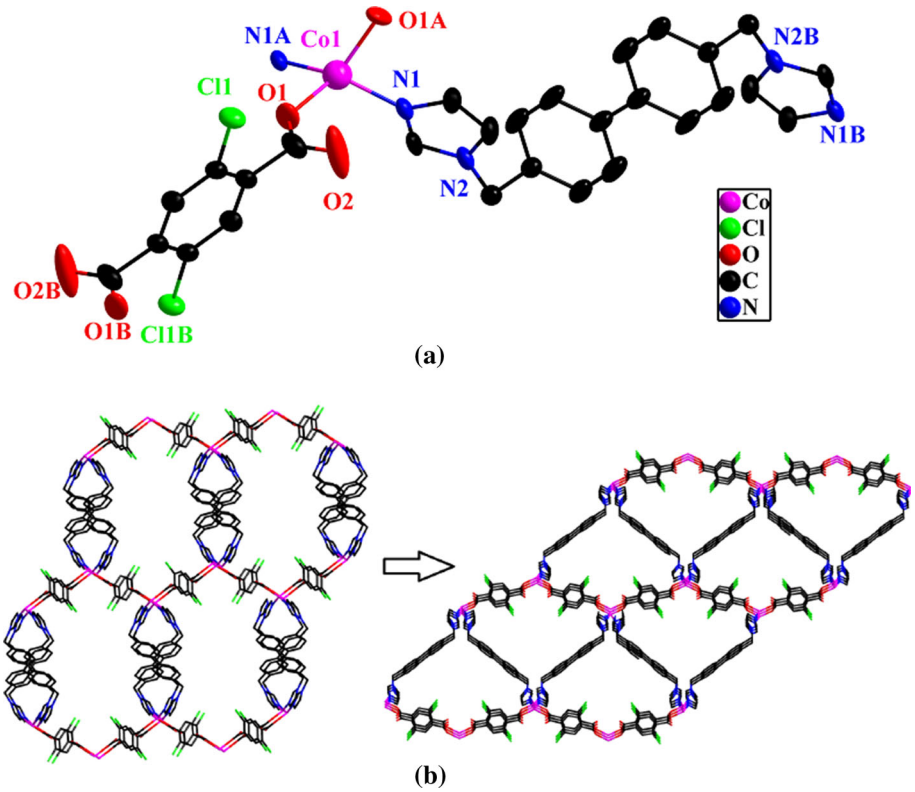

Fig. 2 **a** Coordination environment around the Co(II) centers in the title CP **2**. Hydrogen atoms are omitted for clarity (symmetry codes: A: $-x + 1, y, -z + 3/2$; B: $-x + 1, -y, -z + 1$). **b** A heart-like 3D network constructed by Co(II) centers, L ligands, and $DCTP^{2-}$ ligands

type Class Ia, $Z = 5 \times 1 = 5$ (Zt = 5; Zn = 1), where Zt and Zn are the number of interpenetrated nets related by translation and crystallographic symmetry, respectively [26]. There is no residual solvent accessible void in CP **2** based on a PLATON calculation [27].

To summarize, for CPs **1** and **2**, obvious structural differences are observed in their discrete mononuclear motifs to 3D coordination frameworks, which can be explained by the different metals involved. Thus, the metal centers in these two CPs have different coordination numbers and geometries. For CP **1**, the Ni(II) centers are six-coordinate with an ideal $[NiO_2N_4]$ octahedral geometry, whereas, in CP **2**, the Co(II) centers are four-coordinate with a distorted $[NiO_2N_2]$ tetrahedral geometry. The $DCTP^{2-}$ ligands in both CPs are all unidentate, acting as the spacers to bridge pairs of metal atoms. The $DCTP^{2-}$ ligands are almost perpendicular to the Ni(II) and Co(II) centers, due to the significant steric effects of the chloro substituents. As for ligand L, it serves as either a bridging spacer or as a unidentate terminal ligand in these CPs. Hence, the metal–ligand synergistic effect is essential to modulate the resulting structures.

Spectroscopic powder diffraction studies

The IR spectra for free H_2DCTP, L ligands and the two CPs **1**–**2** are summarized in Table 3. In the IR spectra of both CPs, a band around 1578 cm^{-1} can be attributed to the $\nu_{C=N}$ stretching vibration of the L ligand, while a peak around 660 cm^{-1} can be assigned to the ν_{C-Cl} stretching vibration from the H_2DCTP ligand. There are no strong absorption peaks around 1700 cm^{-1}, suggesting that the carboxylic groups of the H_2DCTP ligands are completely deprotonated in both CPs. The peaks for the carboxylate stretching are at 1352 cm^{-1} for the symmetric mode (ν_s), 1578 cm^{-1} for the asymmetric mode (ν_{as}) for CP **1**; and at 1369 cm^{-1} for ν_s and 1592 cm^{-1} for ν_{as} for CP **2**. The values of $\Delta\nu[\nu_{as}(COO)–\nu_s(COO)]$, 226 and 223 cm^{-1} for **1** and **2**, respectively, imply the monodentate coordination of the carboxyl groups from H_2DCTP in both of these CPs [28].

Table 3 Infrared data of the H_2DCTP, L ligands and CPs **1** and **2**

Compound	H_2DCTP	L	CP **1**	CP **2**
ν_{C-Cl}	670m	–	659m	658m
ν_{N-H}	–	3225w	3033w	2968w
$\nu_{C=N}$	–	1586s	1639m	1520s
$\nu_{C=O}$	1736s	–	1578s	1592s
ν_{C-H}	2956w	2947m	2966m	2924m

S strong, *m* middle, *w* represents weak

XRPD measurements were performed in order to examine the phase purity of bulk samples of CPs **1** and **2**. The obtained patterns are consistent with the simulated

patterns obtained from their single-crystal structures (Fig. S5), confirming the phase purities of the CPs. XRPD patterns of the CPs 2 months later were still in good agreement with the simulated patterns, indicating that these CPs are stable at room temperature.

Thermal properties

Thermogravimetric (TGA) measurements were performed under an N_2 atmosphere on polycrystalline samples of CPs **1** and **2,** and the resulting TGA curves are shown in Fig. 3. The frameworks show good thermal stabilities, being stable up to 278 °C for CP **1** and 239 °C for CP **2**. The TGA curves reveal a weight loss of 23.7% (calcd. 23.6%) for CP **1** at 278–390 °C, and a similar loss of 35.7% (calcd. 35.8%) for CP **2** from 239 to 400 °C, corresponding to the loss of H_2DCTP ligands in both cases. A second weight loss of 68.1% (calcd. 68.3%) for CP **1** took place from 390 to 588 °C, which was ascribed to decomposition of the L ligands. For CP **2**, the corresponding weight loss of 51.7% (calcd. 51.8%) in the range of 400–580 °C was also ascribed to decomposition of L ligands. The remaining residual masses of 8.2% (calcd. 8.1%) for CP **1** are ascribed to NiO, and 12.3% (calcd. 12.4%) for CP **2** corresponds to CoO.

Luminescence properties

CPs with transition metal centers have been investigated for potential luminescence applications [29]. In the present work, the luminescence properties of CPs **1** and **2** were determined in the solid state at room temperature. The emission spectrum of the free ligand L was also investigated under similar experimental conditions, in order to clarify the nature of the luminescence. As shown in Fig. 4a, upon excitation at ca. 250 nm for the free ligand L, an intense emission was observed at ca. 335 nm, which could be assigned to $\pi \rightarrow \pi^*$ or $\pi^* \rightarrow n$ charge transfer [30]. Emission peaks for CPs **1** and **2** were observed at ca. 341 and 355 nm, respectively, with excitations at ca. 260 and 280 nm. Hence, in comparison with the free ligand L, the emission spectra of both CPs are red-shifted, by 6 nm for CP **1**, and 20 nm for CP **2**. The various interactions within CPs networks often influence their emission spectra [31].

UV/Vis diffuse reflectance spectroscopy

The UV–Vis absorption spectra of free L and the two CPs were recorded in the crystalline state at room temperature. As illustrated in Fig. 4b, the free ligand L displays strong absorption bands at 272 nm, which can be attributed to $\pi^* \rightarrow \pi$ transitions. The lower energy bands in the visible region at 547 nm for **1**, and 550 nm (605 nm) for **2** can be ascribed to spin-allowed *d–d* transitions of the d^8 (Ni^{2+}) and d^7 (Co^{2+}) ions, respectively. Strong absorptions around 269 nm for **1**, and 255 nm for **2** can be attributed to LMCT transitions [32] (Fig. 5).

Catalytic degradation properties

Wastewater produced in industrial processes often contains organic compounds which are toxic and not amenable to direct biological treatment [33]. These can include organic dyes, phenols, pesticides, biphenyls, detergents, hydrocarbons, plasticizers, pharmaceuticals and so on. Thus, economical and effective methods are urgently required to degrade organic pollutants in wastewater streams. In this context, advanced oxidation processes (AOPs), especially

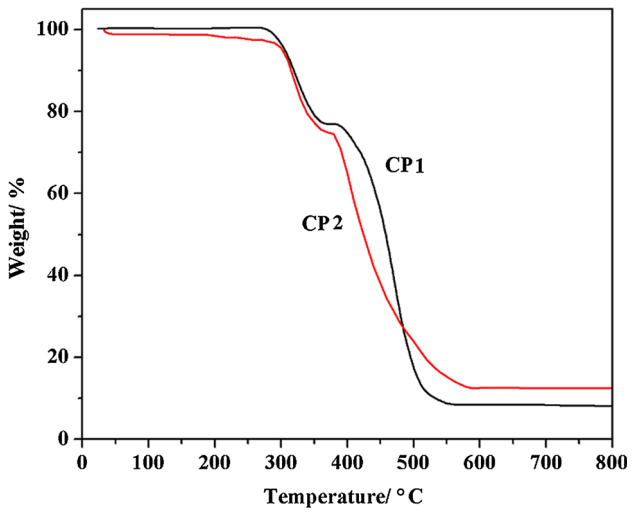

Fig. 3 TGA curves of CPs **1** and **2**

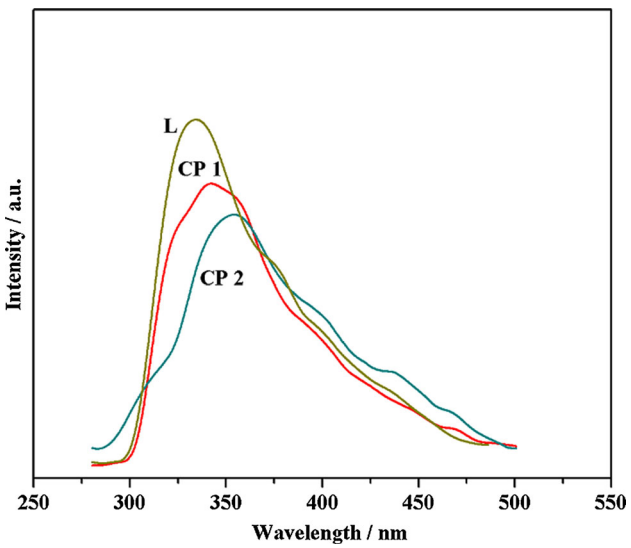

Fig. 4 Solid-state emission spectra of the free ligand L and CPs **1** and **2** at room temperature

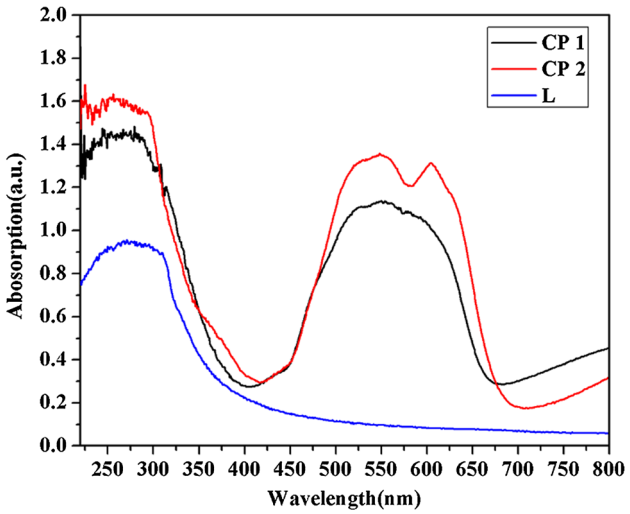

Fig. 5 UV–Vis diffuse reflectance spectra of the free ligand L, and CPs **1** and **2** with $BaSO_4$ as background

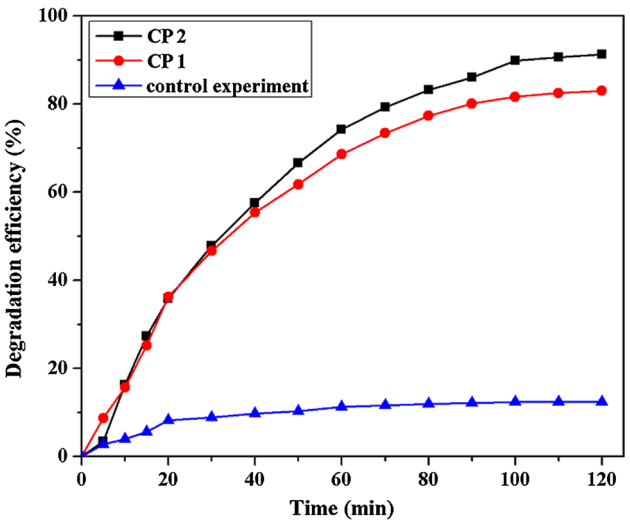

Fig. 6 Experiment results of the catalytic degradation of methyl orange

the Fenton reaction, are attractive on account of their high simplicity, efficiency, and reproducibility [34]. The homogenous Fenton reaction is one of the most environmentally friendly and economical systems. Both Ni(II) and Co(II) centers are able to activate persulfate to produce highly reactive species such as sulfate radicals (SO_4^{-}) and hydroxyl radicals (HO·). These radicals are able to oxidize organic pollutants to CO_2, H_2O and inorganic species [35].

In this work, we chose MO as a model contaminant to assess the efficiency of our CPs as heterogeneous catalysts, with $Na_2S_2O_8$ as the primary oxidant. As illustrated in Fig. 6a, in a control experiment in which only $Na_2S_2O_8$ was added to a solution of MO, the color of MO showed no obvious change after 120 min. The MO degradation in this control experiment reached only 12.43%. On the other hand, when powdered samples of CPs **1** and **2** were added to the solution, the color of MO immediately faded. Thus, the degradation efficiencies reached 83.0% for CP **1**, and 91.2% for CP **2**. The degradation efficiency of CP **1** is lower than that of CP **2**, suggesting that Co-based on CPs may have superior performance for degradation of organic contaminants [36]. In addition, both CPs show better catalytic performance than the previously reported Co(II)/NI(II) CPs [37, 38].

In order to evaluate the stabilities of the two CPs as catalysts for degradation of MO, the experiments were replicated three times under the same conditions. The results showed that both CPs are highly stable under the experimental conditions employed (Fig. S6).

Conclusions

In summary, two new CPs have been prepared and characterized. CP **1** has a 3D network structure with α-Po (or **pcu** net) primitive cubic topology. CP **2** has a 3D framework with the fivefold-interpenetrating **sqc6** topology. The distinct three-dimensional architectures of the two CPs can be attributed to their different metal centers. CP **2** shows promise as a heterogeneous catalyst for degradation of organic pollutants in a Fenton-like process.

Supplementary material

CCDC 1503823-1503824 contain the supplementary crystallographic data for the CPs **1** and **2**. The data can be obtained free of charge via http://www.ccdc.cam.ac.uk/conts/retrieving.html, or from the Cambridge Crystallographic Data Centre, 12 Union Road, Cambridge CB2 1EZ, UK; fax: (+44) 1223-336-033; or e-mail: deposit@ccdc.cam.ac.uk.

Acknowledgements The project was supported by the National Natural Science Foundation of China (51474086), Natural Science Foundation-Steel and Iron Foundation of Hebei Province (B2015209299).

References

1. Bétard A, Fischer RA (2012) Chem Rev 112:1055–1083
2. Cui Y, Yue Y, Qian G, Chen B (2012) Chem Rev 112:1126–1162
3. Dhakshinamoorthy A, Garcia H (2014) Chem Soc Rev 43:5750
4. Xu C, Guo Q, Wang X, Hou H, Fan Y (2011) Cryst Growth Des 11:1869–1879
5. Cook TR, Zheng YR, Stang PJ (2013) Chem Rev 113:734–777
6. Yang L, Powell DR, Houser RP (2007) Dalton Trans 955–964
7. Cohen SM (2012) Chem Rev 112:970–1000
8. Hao SY, Liu YG, Hao ZC, Cui GH (2016) Z Anorg Allg Chem 642:618–625

9. Liu C, Cui GH, Zou KY, Zhao JL, Gou XF, Li ZX (2013) CrystEngComm 15:324
10. Liu D, Lang JP, Abrahams BF (2011) J Am Chem Soc 133:11042–11045
11. Wang XX, Yu B, Van Hecke K, Cui GH (2014) RSC Adv 4:61281–61289
12. Stepanow S, Strunskus T, Lingenfelder M, Dmitriev A, Spillmann H, Lin N, Barth JV, Wöll Ch, Kern K (2004) J Phys Chem B 108:19392–19397
13. Cui GH, He CH, Jiao CH, Geng JC, Blatov VA (2012) CrystEngComm 14:4210–4216
14. DeFuria MD, Zeller M, Genna DT (2016) Cryst Growth Des 16:3530–3534
15. Desmarets C, Poli F, Le Goff XF, Müller K, Amouri H (2009) Dalton Trans 10429–10432
16. Rather B, Zaworotko MJ (2003) Chem Commun 9:830–831
17. Wang C, Zhang T, Lin W (2012) Chem Rev 112:1084–1104
18. Zhang X, Zhao YQ, Wang FS, Dong GY (2016) Chin J Inorg Chem 35:765–773
19. Hao JM, Yu BY, Van Hecke K, Cui GH (2015) CrystEngComm 17:2279–2293
20. Sheldrick GM (1996) Program for empirical absorption correction of area detector data. University of Göttingen, Göttingen
21. Spek A (2009) Acta Cryst D 65:148–155
22. Zhang X, Liu YG, Yu B, Cui GH (2015) Transit Met Chem 41:213–223
23. Wang XL, Li J, Tian AX, Zhao D, Liu GC, Lin HY (2011) Cryst Growth Des 11:3456–3462
24. Blatov V, Shevchenko A (1999) TOPOS 4.0. Samara State University, Samara Oblast
25. Hu JM, Blatov VA, Yu B, Van Hecke K, Cui GH (2016) Dalton Trans 45:2426–2429
26. Shi Z, Pan Z, Jia H, Chen S, Qin L, Zheng H (2016) Cryst Growth Des 16:2747–2755
27. Sheldrick GM (2014) Program for X-ray crystal structure determination. Göttingen University, Göttingen
28. Yin HD, Hong M, Wang QB, Xue SC, Wang DQ (2005) J Organomet Chem 690:1669–1676
29. Hu Z, Deibert BJ, Li J (2014) Chem Soc Rev 43:5815
30. Kuritz N, Stein T, Baer R, Kronik L (2011) J Chem Theory Comput 7:2408–2415
31. Allendorf M, Bauer C, Bhakta R, Houk R (2009) Chem Soc Rev 38:1330–1352
32. Lampeka YD, Gavrish SP (2000) Polyhedron 19:2533–2538
33. Dai M, Li HX, Lang JP (2015) CrystEngComm 17:4741–4753
34. Wu XY, Qi HX, Ning JJ, Wang JF, Ren ZG, Lang JP (2015) Appl Catal B 168:98–104
35. Sun H, Wang S (2015) RSC Catal 27:209–247
36. Wang X, Huang J, Liu L, Liu G, Lin H, Zhang J, Chen N, Qu Y (2013) RSC Adv 3:13944
37. Jiao CH, He CH, Geng JC, Cui GH (2011) Transit Met Chem 37:17–23
38. Hao JM, Zhao YN, Yu BY, Van Hecke K, Cui GH (2014) Transit Met Chem 39:741–753